High power all-fiberized and narrow-bandwidth MOPA system by tandem pumping strategy for thermally induced mode instability suppression

Pengfei Ma[1,2], Hu Xiao[1,2], Daren Meng[1], Wei Liu[1], Rumao Tao[1,2], Jinyong Leng[1,2], Yanxing Ma[1,2], Rongtao Su[1,2], Pu Zhou[1,2], and Zejin Liu[1,2]

[1]*College of Advanced Interdisciplinary Studies, National University of Defense Technology, Changsha 410073, China*

[2]*Hunan Provincial Collaborative Innovation Center of High Power Fiber Laser, National University of Defense Technology, Changsha 410073, China*

Abstract

An all-fiberized and narrow-bandwidth master oscillator power amplification (MOPA) system with record output power of 4 kW level and slope efficiency of 78% is demonstrated. Tandem pumping strategy is tentatively introduced into the narrow-bandwidth MOPA system for thermally induced mode instability (TMI) suppression. The stimulated Brillouin scattering (SBS) effect is balanced by simply using one-stage phase modulation technique. With different phase modulation signals, SBS limited output powers of 336 W, 1.2 kW and 3.94 kW are respectively achieved with spectral bandwidths accounting for 90% power of ∼0.025, 0.17 and ∼0.89 nm. Compared with our previous 976 nm pumping system, TMI threshold is overall boosted to be >5 times in which tandem pumping increases the TMI threshold of >3 times. The beam quality (M^2 factor) of the output laser is well within 1.5 below the TMI threshold while it is ultimately saturated to be 1.86 with the influence of TMI at maximal output power. Except for SBS and TMI, stimulated Raman scattering (SRS) effect will be another challenge for further power scaling. In such a high power MOPA system, multi-detrimental effects (SBS, SRS and TMI) will coexist and may be mutual-coupled, which could provide a well platform for further comprehensively investigating and optimizing the high power, narrow-bandwidth fiber amplifiers.

Keywords: advanced laser technology and applications; design; fiber laser and applications; high power laser; laser amplifiers; laser systems; modeling; narrow linewidth; optimization

1. Introduction

High power fiber laser sources with near-diffraction-limited beam quality have been strongly required in many scientific and industrial applications[1–3]. However, power scaling of the monolithic fiber laser system has been challenged as a result of the limitations of nonlinear effects, fiber damage, high brightness pump sources and thermally induced mode instability (TMI)[4–6]. Coherent and spectral beam combining systems are the two alternatively brightness-maintained approaches to break through the power scaling limitations of the monolithic fiber laser/amplifier[7–10]. In coherent and spectral beam combining systems, high brightness fiber amplifier with characteristic of narrow bandwidth is their basic unit, which tightly determines the power scaling ability of the beam combining systems. Traditional studies show that output power of this type of fiber source is mainly restricted by the effects of nonlinear stimulated Brillouin scattering (SBS) and/or TMI[4–6].

As for SBS effect, some effective approaches had been proposed to mitigate its influence over the past decade. These approaches mainly include incorporating thermal and longitudinal stress gradients[11–13], using counter-propagating pump[14], special transverse-designed active fiber[12, 15], multi-longitudinal-mode fiber oscillator[16, 17], filtered super-fluorescent source[10, 18], multi-wavelength injection and laser gain competition[19, 20] and applying phase modulation technique[8, 9, 20–29]. Within these SBS management approaches, phase modulation technique is a preferable approach beyond the output power of multi-kilowatt level[22–29]. As for TMI effect, several potential

Correspondence to: P. Ma and P. Zhou, College of Advanced Interdisciplinary Studies, National University of Defense Technology, Changsha 410073, China. Email: zhoupu203@163.com (P. Zhou); shandapengfei@126.com (P. Ma).

suppressing methods had also been proposed and validated by investigating on its physical mechanism[30–37]. Generally, TMI effect could be suppressed by optimizing the doping area or imposing external bend loss of higher-order modes for mode selection[23–26, 30–33], reducing the core size or numerical aperture (NA) of the active fiber[27, 28, 31, 34], increase of the seed power[33], weakening head load by optimizing the injected ratios of co-pumped and counter-pumped laser[33, 35, 36], decrease of quantum defect and/or pump absorption[33, 35, 37]. Nowadays, as high as 3 kW and 3.5 kW output powers with narrow bandwidths and near-diffraction-limited beam qualities had been respectively presented by using gold-coated specialty gain fiber[24] and low-NA active fiber[28], while the configurations are not all-fiberized and some bulk space components were employed. As for all-fiberized formats, as high as ∼2.5 kW power level had been reported both in nonpolarization-maintained and polarization-maintained fiber amplifiers[25, 26, 29].

Despite most of the high power, narrow-bandwidth fiber amplifiers being pumped by 976 nm laser diodes (LDs) for being favorable of SBS management, tandem pumping is a robust route for simultaneously decreasing the quantum defect and pump absorption for TMI suppression[33, 37]. This technique had been widely used in high power fiber amplifiers with broadband spectral characteristics[38–42], and the output powers had been remarkably scaled to be beyond 3.5 kW power level by several groups[38, 41, 42]. Due to the small absorption area of the Yb-doped active fiber at 1018 nm, one point should be noted that the suppressions of SBS and stimulated Raman scattering (SRS) are more difficult when tandem pumping is employed in high power, narrow-bandwidth fiber amplifiers.

In this manuscript, we tentatively introduce tandem pumping strategy for TMI suppression in a 4 kW power level narrow-bandwidth and all-fiberized amplifier. In order to further suppress SBS effect, one-stage phase modulation with large amplitude sinusoid or white noise signals (WNSs) is employed. SBS limited output powers of 336 W, 1.2 kW and 3.94 kW are obtained with spectral bandwidths accounting for 90% power of ∼0.025, 0.18 and ∼0.89 nm, respectively. Compared with our previous 976 nm pumping system, TMI threshold is overall enhanced to be >5 times and the contribution of tandem pumping could be as high as >3 times. The residual TMI threshold enhancement is contributed to the increase of the seed power. The M^2 factor is measured to be within 1.5 below the TMI threshold and it is ultimately saturated to be 1.86 with the impact of TMI effect.

2. Experimental setup

The experimental setup of the high power tandem-pumped, narrow-bandwidth and all-fiberized fiber amplifier is shown in Figure 1, which is based on a typical master oscillator power amplification (MOPA) format. The seed laser (Seed) is a low noise, strictly single-frequency (linewidth <20 kHz) fiber laser constructed by an ultrashort cavity with high gain phosphate glass active fiber[43]. The output power of the Seed is measured to be 60 mW with central wavelength of 1064.4 nm. First, the spectral bandwidth of the seed laser is broadened by using one-stage phase modulation system for SBS suppression, which consists of a signal generator and a phase modulator (PM). In the experiment, large amplitude sinusoid or filtered WNSs with different electronic bandwidths and modulation depths are alternatively employed. The insertion loss of the PM is about 3 dB and the output power after PM is ∼30 mW. After PM, the laser power is pre-amplified by using three-stage all-fiberized pre-amplifiers (P-AI, P-AII, P-AIII). P-AI is a core-pumped pre-amplifier with ∼0.8 m highly doped (pump absorption coefficient ∼250 dB/m @ 976 nm), single-clad Yb-doped active fiber (YDF, core/cladding diameter ratio of ∼6/125 μm). LD1 with maximal output power of 480 mW and central wavelength of 976 nm is employed to pump the active fiber via a wavelength division multiplexer (WDM). The output power could be scaled to ∼150 mW after an isolator (ISO1) to block off the backward power. P-AII and P-AIII are two cladding-pumped pre-amplifiers. As for P-AII, LD2 with maximal output power of ∼9 W and central wavelength of 974 nm is used to pump 3.5 m long active fiber (YDF-I, pump absorption coefficient ∼4 dB/m @ 975 nm) via a (2+1)×1 combiner. The core and cladding diameters of the active fiber are 10 μm and 125 μm, respectively. After P-AII, the output power is boosted to ∼3 W after ISO2. For P-AIII, the active fiber (YDF-II) is pumped by using two wavelength-stabilized laser diodes (LD3, LD4) with maximal output power of ∼90 W and central wavelength of 976 nm via a (2+1)×1 combiner. The core and cladding diameters of the active fiber are 15 μm and 130 μm, respectively, and 2.8 m long active fiber with pump absorption coefficient of ∼5.4 dB/m @ 976 nm is used. After P-AIII, the output power is further scaled to ∼70 W after ISO3. At the rear end port of P-AIII, a fiber coupler (C) is incorporated into the MOPA system. The coupling ratios of the out port of C to signal port and backward monitor (BM) port are 99.9% and 0.1%, respectively. 0.1% port is used for diagnosing the SBS effect and ensuring the safety of the whole MOPA system during the power scaling process.

The final amplifier is pumped by using three 2 kW power level 1018 nm all-fiberized lasers via a (6 + 1) × 1 combiner. Each 2 kW level 1018 nm pump laser is constructed by power combining of seven 300 W level 1018 nm single mode fiber lasers via a homemade 7 × 1 all-fiberized power combiner[44]. The active fiber used in this amplifier is large mode area and double clad Yb-doped fiber (YDF-III) with a core diameter of 30 μm and an inner cladding diameter of 250 μm. The pump absorption coefficient is measured to
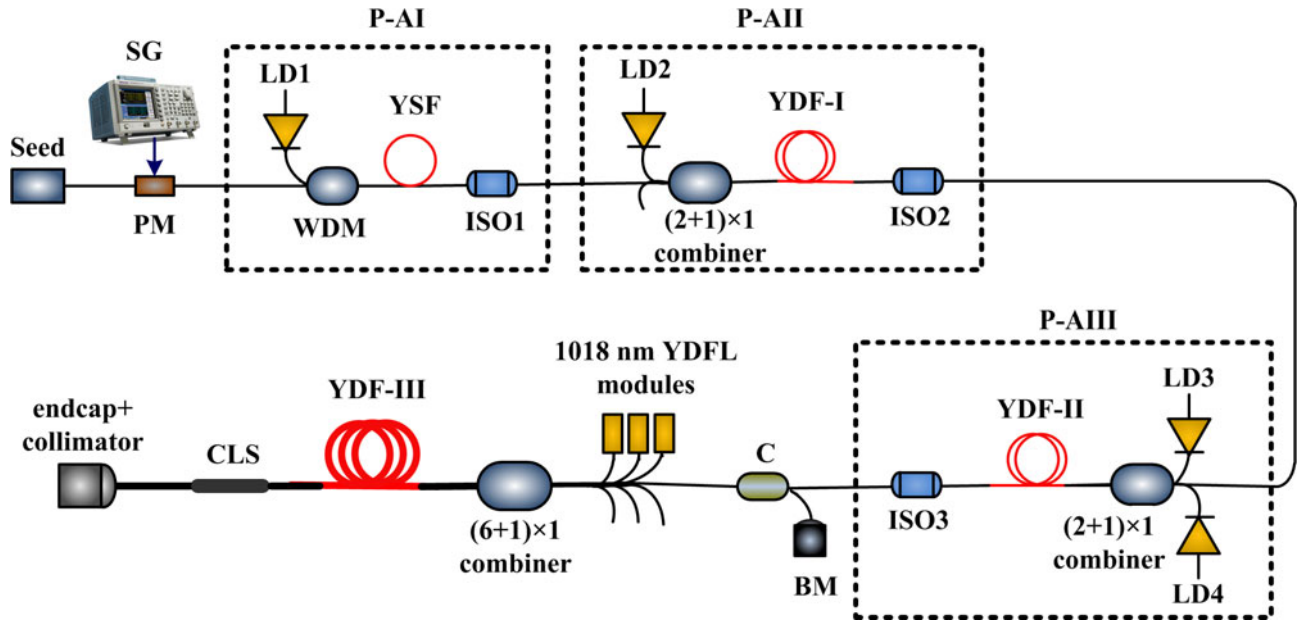
Figure 1. Experimental setup of high power tandem-pumped, narrow-bandwidth and all-fiberized fiber amplifier.
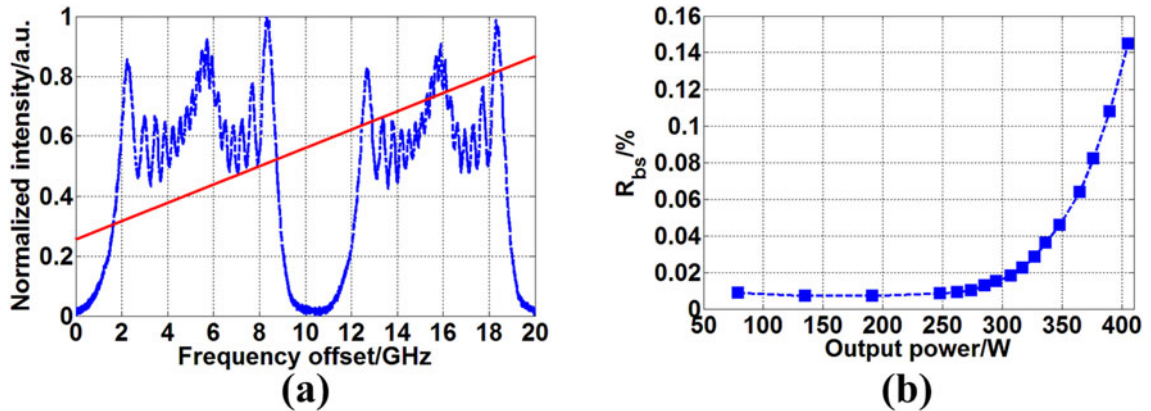

Figure 2. (a) The measured spectral distribution of the phase modulated laser; (b) the trend of backward power ratio (R_{bs}) along with power scaling.

be ~0.5 dB/m @ 1018 nm and ~31 m long active fiber is employed for high power amplification. The amplified laser is successively delivered through homemade cladding light stripper (CLS), fiber endcap and collimator to free space.

3. Experimental results and discussions

3.1. Power scaling of large amplitude sinusoid signal modulated seed

For achieving the criteria of SBS threshold at relatively safety state, we first investigate the power scaling process and SBS suppressing effect by using large amplitude sinusoid signal for phase modulation. The amplitude and repetition rate of the phase modulated signal are set to be 50 V and 100 MHz, respectively. The typical half-wave voltage

and electro-optic bandwidth within 1 dB of the PM used in this section are 2 V @ 50 kHz and 150 MHz, respectively. The spectral distribution of the phase modulated laser is shown in Figure 2(a) and the trend of backward power ratio (R_{bs}) along with power scaling is shown in Figure 2(b). The spectral distribution is measured by using a Fabry–Perot interferometer (FPI) with free spectral range (FSR) of 10 GHz and resolution limit of about ~68 MHz. R_{bs} is defined as the ratio of actual backward power to the output power. The actual backward power is calculated by dividing the backward coupling ratio (0.1%) by the collected power values of BM. As shown in Figure 2(a), the spectral range is well within 10 GHz by using large amplitude sinusoid signal modulation. Since the spectral distribution by phase modulation is normally irregular, the spectral range accounting for 90% power is defined as the spectral bandwidth in all the following cases. This spectral
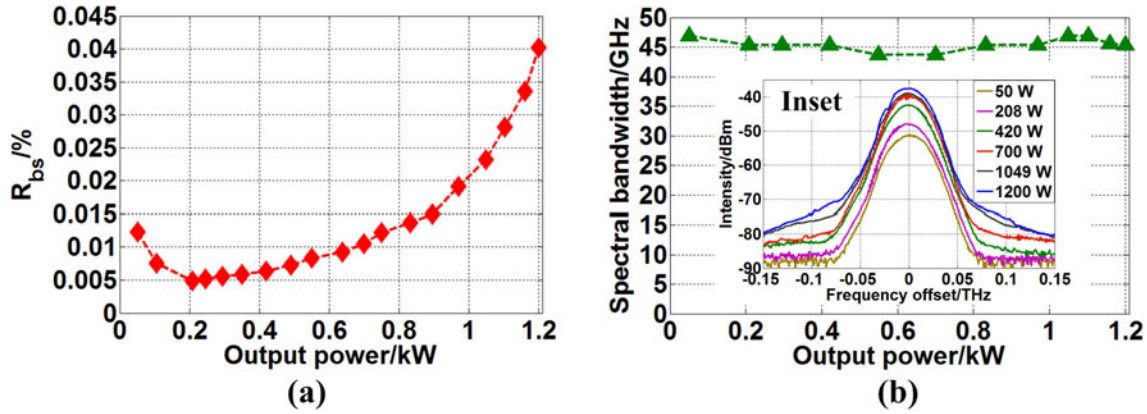
Figure 3. (a) The change of R_{bs} along with output power; (b) the spectral bandwidth as a function of output power (inset: the frequency offset distributions at different output powers).

bandwidth criterion is conservative for both coherent and spectral beam combining systems design. By calculation, the spectral bandwidth is about 6.6 GHz (0.025 nm). As shown in Figure 2(b), when the output power is beyond ∼336 W, R_{bs} exponentially increases along with power scaling, which corresponds to an R_{bs} inflection value of ∼ 0.04%. This R_{bs} inflection value is defined as the criteria of SBS threshold in the following experiments.

### 3.2. Power scaling of filtered 2 GHz–WNS modulated seed

In this section, we investigate the power scaling process and SBS suppressing effect by using filtered WNS signal with 2 GHz electronic bandwidth for phase modulation. The broadband electronic WNS signal is first filtered by using an electronic low-pass filter and then amplified to an amplitude of 4.5 V for phase modulation and spectral broadening. The typical half-wave voltage of the PM used in this case is 2.7 V @ 1 GHz, and the electro-optic bandwidth at 2 dB is about 15 GHz. The increase of R_{bs} (%) along with power scaling process is shown in Figure 3(a), which shows that SBS limited output power of ∼1.2 kW could be achieved in this case. Figure 3(b) shows the change of spectral bandwidth as a function of output power scaling, and the inset in Figure 3(b) gives the frequency offset (THz) distributions of the amplified laser at several different output powers. As shown in Figure 3(b), the spectral bandwidth broadens little along with the increase of the output power. Inset shown in Figure 3(b) denotes that Gaussian-like spectra with well symmetry are generated by the spectral broadening system. The measured spectral bandwidth is just ∼45 GHz (∼0.17 nm) at 1.2 kW power level. Besides, by analysis, the full width at half maximum (FWHM) of the spectral range is also broadened little with the increase of the output power. In the experiment, the essential reason for avoiding spectral broadening is that the temporal characteristic of the single-frequency seed laser is quite stable and self-phase-modulation effect induced noise transfer from intensity to phase is weak[45]. At the maximal output power, the FWHM of the spectral range is ∼31 GHz (∼0.12 nm).

3.3. Power scaling of filtered 12 GHz–WNS modulated seed

For further SBS management, an electronic low-pass filter with 12 GHz electronic bandwidth is used for phase modulation and spectral broadening. The filtered WNS is amplified to an amplitude of 5 V. The type of PM used in this situation is identical as shown in Section 3.2. Figure 4(a) shows the power scaling process of the MOPA system along with the increase of pump power, which indicates a slope efficiency of 78% and a well linear-fitting trend. With injected pump power of 5057 W, 3940 W output power is ultimately achieved. The increase of R_{bs} (%) as a function of the output power is shown in Figure 4(b), which denotes that SBS threshold is about ∼3.9 kW. At 3940 W, the backward power ratio (R_{bs}) is measured to be 0.046%.

With the increase of output power, the change of spectral bandwidth is shown in Figure 5(a) and the frequency offset (THz) of the emitted laser at different output powers is shown in the inset of Figure 5(a). From Figure 5(a), it could be inferred that the spectral bandwidth fluctuates between 0.245 THz and 0.205 THz in the whole power scaling process. The fluctuation phenomenon of spectral bandwidth is attributed to the spectral asymmetry of the amplified laser, as shown in the inset of Figure 5(a). The spectral asymmetry of the amplified laser is mainly caused by the comprehensive effects of limited electro-optic bandwidth of the PM and gain competitions in the whole amplifications. The sideband broadening is contributed to self-phase-modulation and four-wave-mixing effects[45, 46]. At the maximal output power, the spectral bandwidth is measured to be 0.237 THz (0.89 nm). It should be noted that the time-coherence control of such a spectral bandwidth had been successfully fulfilled in 2 kW level coherent beam combining structure[8]. Compared with the spectral bandwidth (0.245 THz) of the injected seed (50 W power
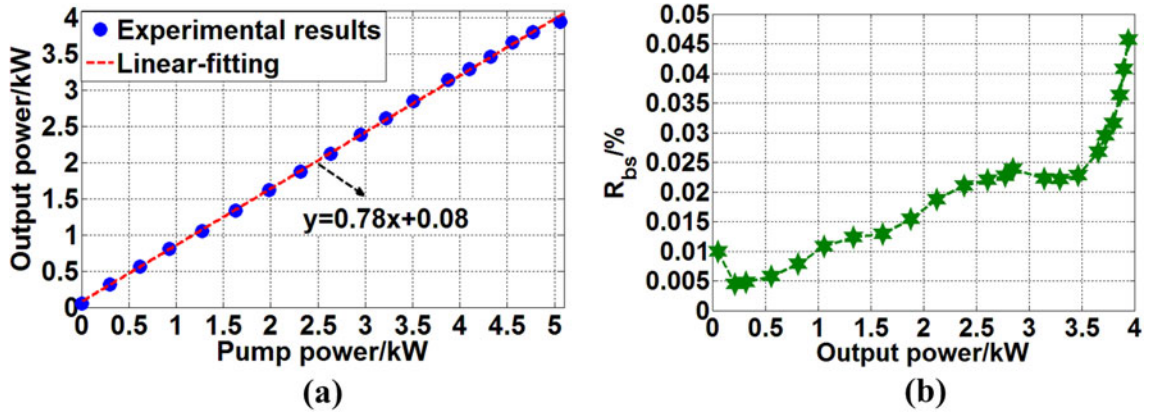
Figure 4. (a) The power scaling process of the MOPA system along with increase of pump power; (b) the increase of R_{bs} (%) as a function of the output power.
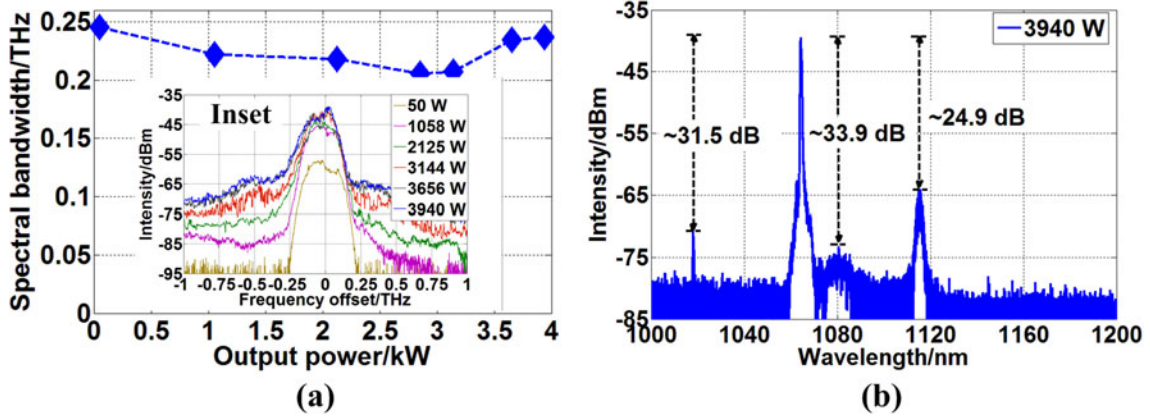

Figure 5. (a) The change of spectral bandwidth with the output power (inset: the frequency offset at several different output powers); (b) the spectrum from 1000 to 1200 nm at 3940 W.

level), it broadens little when the output power boosts to be 3940 W. Figure 5(b) is the spanned emission spectrum from 1000 to 1200 nm at 3940 W. The signal to noise ratio (SNR) of the signal laser is ~31.5 dB, ~33.9 dB and ~24.9 dB compared with the residual 1018 nm pump laser, amplified spontaneous emission and Raman Stokes light, respectively. Except for SBS effect, SRS will be another challenge for further power scaling of such high power, tandem-pumped fiber laser systems.

Along with power scaling, the intensity signal and the corresponding Fourier spectral distribution are diagnosed by using an oscilloscope with 1 GHz bandwidth and an InGaAs photo-detector (PD) with 150 MHz electro-optic bandwidth. In the experiment, when the output power scales from 2205 W to 2253 W, a sudden intensity noise is observed in the PD-captured intensity distribution. The normalized intensity signals collected by the PD at 2205 W, 2253 W and 3940 W are depicted in Figure 6(a). By analysis, the standard deviations of the intensity signals are jumped from 1.38% to 2.5% when the output power increases from 2205 W to 2253 W. The standard deviation of the intensity signal is saturated to be 2.8% at 3940 W. Figure 6(b) shows the corresponding Fourier spectral distributions of the intensity signals at 2205 W, 2253 W and 3940 W. Compared with

the Fourier spectral distribution at output power of 2205 W, noise-like protuberance exists within the frequency range from 0 to 5 kHz at output power of 2253 W. At 3940 W, the frequency range of noise-like protuberance is extended from 0 to ~20 kHz. By combining temporal–spectral characteristics of TMI[47, 48], it is confirmed that the TMI effect occurs when the output power is beyond 2253 W. Further, the beam quality (M^2 factor) of the amplified laser is examined along with power enhancement, which is shown in Figure 6(c). From Figure 6(c), it is concluded that the M^2 factor is well within 1.5 below the TMI threshold. The M^2 factor is transited to 1.55 at 2253 W and abruptly deteriorates to 1.88 at 2384 W. For further power scaling, the M^2 factor is nearly maintained and saturated and it is measured to be 1.86 at 3940 W. Figure 6(d) shows the typical far-field beam profiles at different output powers. From Figure 6(d), it can be seen that the beam profile is near Gaussian-like with an output power of 1878 W (below TMI threshold). At TMI threshold (2253 W), some extent of distortion could be observed. For further power scaling to 2384 W, 2775 W and 3000 W, the beam profiles are distorted seriously and obvious higher-order modes could be observed. For further power scaling to 3940 W, the TMI has been transmitted to chaotic state and
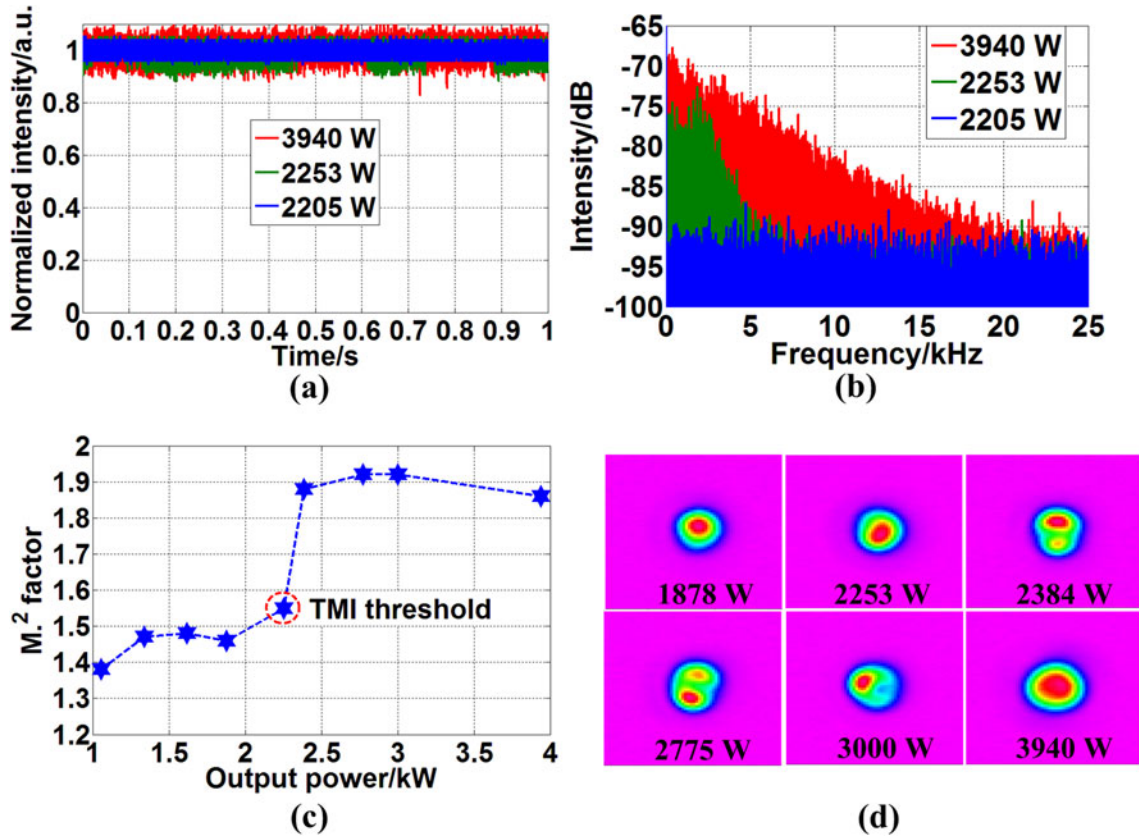
Figure 6. (a) The normalized intensity signals collected by PD; (b) the corresponding Fourier spectral distributions; (c) the measured M^2 factor along with power enhancement; (d) the typical far-field beam profiles at different output powers.

the beam profile is the superposition of fundamental mode and higher-order modes.

As shown above, the TMI threshold is measured to be ∼2253 W by using tandem pumping strategy. This TMI threshold is higher than 5 times compared with our previous result (TMI threshold ∼446 W) in which the identical type of active fiber was pumped by 976 nm LDs and ∼10 W pre-amplified seed power was injected into the main amplifier for final power amplification[49]. By theoretical analysis based on a self-built model[33], 1018 nm tandem pumping manner could scale the TMI threshold of 3.2 times compared with 976 nm pumping case. Increase of the injected power from 10 W to 70 W could scale the TMI threshold of 1.4 times. By employing tandem-pumping-suitable active fiber for higher TMI threshold at 976 nm, higher output power with near-diffraction-limited beam quality could be expected.

4. Conclusions

In this work, we demonstrate a record 4 kW power level all-fiberized, narrow-bandwidth MOPA system by using tandem pumping for TMI management. The SBS effect is balanced by using one-stage phase modulation technique for moderate spectral broadening. The SBS suppressing effects of large amplitude sinusoid signal and filtered WNSs

are investigated. By defining the spectral offset range accounting for 90% power as the spectral bandwidth, SBS limited output powers of 336 W, 1.2 kW and 3.94 kW are respectively achieved with bandwidth of ∼0.025 nm (6.6 GHz), 0.17 nm (45 GHz) and ∼0.89 nm (0.237 THz). The TMI suppressing ability of this MOPA system is compared with our previous 976 nm pumped format, which indicates that TMI threshold is scaled to >5 times. By analysis, the 1018 nm tandem pumping could boost the threshold of ∼3.2 times and the increase of injected seed power could enhance the threshold of 1.4 times. The M^2 factor of the amplified laser is well within 1.5 below the TMI threshold and it is ultimately saturated to be 1.86 with the impact of TMI at 3940 W. Further output power scaling is limited by the comprehensive effects of SBS, TMI and SRS, which will provide a well platform for investigating the mutual-coupled effects among the above three detrimental factors and the possible optimizing strategies for higher power, narrow-bandwidth fiber amplifiers.

References

1. D. J. Richardson, J. Nilsson, and W. A. Clarkson, J. Opt. Soc. Am. B **27**, B63 (2010).
2. M. N. Zervas and C. A. Codemard, IEEE J. Sel. Top. Quantum Electron. **20**, 0904123S (2014).
3. W. Shi, Q. Fang, X.-S. Zhu, R. Norwood, and N. Peyghambarian, Appl. Opt. **53**, 6554 (2014).
4. J. W. Dawson, J. M. Messerly, R. J. Beach, M. Y. Shverdin, E.A. Stappaerts, A. K. Sridharan, P. H. Pax, J. E. Heebner, C. W. Siders, and C. P. J. Barty, Opt. Express **16**, 13240 (2008).
5. H. Otto, C. Jauregui, J. Limpert, and A. Tünnermann, Proc. SPIE **9728**, 97280E (2016).
6. M. Zervas, Proc. SPIE **10512**, 1051205 (2018).
7. T. Y. Fan, IEEE J. Sel. Top. Quantum Electron. **11**, 567 (2005).
8. Z.-J. Liu, P.-F. Ma, R.-T. Su, R.-M. Tao, Y.-X. Ma, X.-L. Wang, and P. Zhou, J. Opt. Soc. Am. B. **34**, A7 (2016).
9. I. Dajani, A. Flores, R. Holten, B. Anderson, B. Pulford, and T. Ehrenreich, Proc. SPIE **9728**, 972801 (2016).
10. Y. Zheng, Y.-F. Yang, J.-H. Wang, M. Hu, G.-B. Liu, X. Zhao, X.-L. Chen, K. Liu, C. Zhao, B. He, and J. Zhou, Opt. Express **24**, 12064 (2016).
11. L. Huang, H.-S. Wu, R.-X. Li, L. Li, P.-F. Ma, X.-L. Wang, J.-Y. Leng, and P. Zhou, Opt. Lett. **42**, 1 (2017).
12. C. Robin, I. Dajani, and B. Pulford, Opt. Lett. **39**, 666 (2014).
13. L. Zhang, S.-Z. Cui, C. Liu, J. Zhou, and Y. Feng, Opt. Express **21**, 5456 (2013).
14. T. Theeg, H. Sayinc, J. Neumann, and D. Kracht, IEEE Photon. Tech. Lett. **24**, 1864 (2012).
15. S. Gray, A. Liu, D. Walton, J. Wang, M. Li, X. Chen, A. Ruffin, J. Demeritt, and L. Zenteno, Opt. Express **15**, 17044 (2007).
16. Y. Xu, Q. Fang, Y.-G. Qin, X.-J. Meng, and W. Shi, Appl. Opt. **54**, 9419 (2015).
17. Z.-H. Huang, X.-B. Liang, C.-Y. Li, H.-H. Lin, Q. Li, J.-J. Wang, and F. Jing, Appl. Opt. **55**, 297 (2016).
18. J.-M. Xu, W. Liu, J.-Y. Leng, H. Xiao, S.-F. Guo, P. Zhou, and J.-B. Chen, Opt. Lett. **40**, 2973 (2015).
19. P. Weßels, P. Adel, M. Auerbach, D. Wandt, and C. Fallnich, Opt. Express **12**, 4443 (2004).
20. N. Naderi, A. Flores, B. Anderson, and I. Dajani, Opt. Lett. **41**, 3964 (2016).
21. A. V. Harish and J. Nilsson, IEEE J. Sel. Top. Quantum Electron. **24**, 5100110 (2018).
22. A. Flores, C. Robin, A. Lanari, and I. Dajani, Opt. Express **22**, 17735 (2014).
23. P.-F. Ma, R.-M. Tao, R.-T. Su, X.-L. Wang, P. Zhou, and Z.-J. Liu, Opt. Express **24**, 4187 (2016).
24. C. X. Yu, O. Shatrovoy, T. Y. Fan, and T. F. Taunay, Opt. Lett. **41**, 5202 (2016).
25. M. Kanskar, J. Zhang, J. Koponen, O. Kimmelma, V. Aallos, I-Ning Hu, and A. Galvanauskas, Proc. SPIE **10512**, 105120F (2018).
26. R.-T. Su, R.-M. Tao, X.-L. Wang, H.-W. Zhang, P.-F. Ma, P. Zhou, and X.-J. Xu, Laser Phys. Lett. **14**, 085102 (2017).
27. K. Brar, M. Savage-Leuchs, J. Henrie, S. Courtney, C. Dilley, R. Afzal, and E. Honea, Proc. SPIE **8961**, 89611R (2014).
28. F. Beier, C. Hupel, S. Kuhn, S. Hein, J. Nold, F. Proske, B. Sattler, A. Liem, C. Jauregui, J. Limpert, N. Haarlammert, T. Schreiber, R. Eberhardt, and A. Tünnermann, Opt. Express **25**, 14892 (2017).
29. N. Platonov, R. Yagodkin, J. D. L. Cruz, A. Yusim, and V. Gapontsev, Proc. SPIE **10512**, 105120E (2018).
30. A. V. Smith and J. J. Smith, Opt. Express **19**, 10180 (2011).
31. B. Ward, C. Robin, and I. Dajani, Opt. Express **20**, 11407 (2012).
32. M. Laurila, M. Jørgensen, K. Hansen, T. Alkeskjold, J. Broeng, and J. Lægsgaard, Opt. Express **20**, 5742 (2012).
33. R.-M. Tao, X.-L. Wang, and P. Zhou, IEEE J. Sel. Top. Quantum Electron. **24**, 0903319 (2018).
34. C. Jauregui, T. Eidam, H. Otto, F. Stutzki, F. Jansen, J. Limpert, and A. Tünnermann, Opt. Express **20**, 12912 (2012).
35. A. Smith and J. Smith, Opt. Express **21**, 15168 (2013).
36. Z. Eznaveh, G. Galmiche, E. Lopez, and R. Correa, Proc. SPIE **9344**, 93442G (2015).
37. C. Jauregui, H. Otto, F. Stutzki, F. Jansen, J. Limpert, and A. Tünnermann, Opt. Express **21**, 19375 (2013).
38. D. J. Richardson, J. Nilsson, and W. A. Clarkson, J. Opt. Soc. Am. B **27**, B63 (2010).
39. C. Wirth, O. Schmidt, A. Kliner, T. Schreiber, R. Eberhardt, and A. Tünnermann, Opt. Lett. **36**, 3061 (2011).
40. H. Xiao, J.-Y. Leng, H.-W. Zhang, L. Huang, J.-M. Xu, and P. Zhou, Appl. Opt. **54**, 8166 (2015).
41. P. Zhou, H. Xiao, J.-Y. Leng, J.-M. Xu, Z.-L. Chen, H.-W. Zhang, and Z.-J. Liu, J. Opt. Soc. Am. B. **34**, A29 (2017).
42. P. Yan, X.-J. Wang, Z.-H. Wang, Y.-S. Huang, D. Li, Q.-R. Xiao, and M.-L. Gong, IEEE J. Sel. Top. Quantum Electron. **24**, 0902506 (2018).
43. S.-H. Xu, Z.-M. Yang, W.-N. Zhang, X.-M. Wei, Q. Qian, D.-D. Chen, Q.-Y. Zhang, S.-X. Shen, M.-Y. Peng, and J.-R. Qiu, Opt. Lett. **36**, 3708 (2011).
44. R.-X. Li, H. Xiao, J.-Y. Leng, Z.-L. Chen, J.-M. Xu, J. Wu, and P. Zhou, Laser Phys. Lett. **14**, 125102 (2017).
45. W. Liu, W.-J. Kuang, M. Jiang, J.-M. Xu, P. Zhou, and Z.-J. Liu, Laser Phys. Lett. **13**, 035105 (2016).
46. A. G. Kuznetsov, E. V. Podivilov, and S. A. Babin, J. Opt. Soc. Am. B **29**, 1231 (2012).
47. H. Otto, F. Stutzki, F. Jansen, T. Eidam, C. Jauregui, J. Limpert, and A. Tünnermann, Opt. Express **20**, 15710 (2012).
48. I.-N. Hu, C. Zhu, C. Zhang, A. Thomas, and A. Galvanauskas, Proc. SPIE **8601**, 860109 (2013).
49. R.-M. Tao, P.-F. Ma, X.-L. Wang, P. Zhou, and Z.-J. Liu, J. Opt. **18**, 065501 (2016).